Analysis of Nonlinear Multi-Body Systems with Elastic Couplings *

Olivier A. Bauchau and Dewey H. Hodges
Georgia Institute of Technology,
School of Aerospace Engineering.
Atlanta, Georgia, 30332, USA.

Abstract

This paper is concerned with the dynamic analysis of nonlinear multi-body systems involving elastic members made of laminated, anisotropic composite materials. The analysis methodology can be viewed as a three-step procedure. First, the sectional properties of beams made of composite materials are determined based on an asymptotic procedure that involves a two-dimensional finite element analysis of the cross-section. Second, the dynamic response of nonlinear, flexible multi-body systems is simulated within the framework of energy-preserving and energy-decaying time integration schemes that provide unconditional stability for nonlinear systems. Finally, local three-dimensional stresses in the beams are recovered, based on the stress resultants predicted in the previous step. Numerical examples are presented and focus on the behavior of multi-body systems involving members with elastic couplings.

Keywords: Flexible multi-body systems; Composite materials; Elastic couplings.

1 Introduction

This paper is concerned with the dynamic analysis of flexible, nonlinear multi-body systems, *i.e.* a collection of bodies in arbitrary motion with respect to each other while each body is undergoing large displacements and rotations with respect to a frame of reference attached to the body. The strain within each elastic body is assumed to remain small. The paper focuses on structures made of laminated composite materials and exhibiting elastic couplings.

The elastic bodies are modeled using the finite element method. The use of beam elements will be demonstrated for multi-body systems. The location of each node is represented by its Cartesian coordinates in an inertial frame, and the rotation of the cross-section at each node is represented by a finite rotation tensor expressed in the same inertial frame. The kinematic constraints among the various bodies are enforced via the Lagrange multiplier

* *Multibody System Dynamics*, **3**, 1999, pp 168-188.

technique. Although this approach does not involve the minimum set of coordinates, it allows a modular development of finite elements for the enforcement of the kinematic constraints.

The equations of motion resulting from the modeling of multi-body systems with the above methodology present distinguishing features: they are stiff, nonlinear, differential-algebraic equations. The stiffness of the system stems not only from the presence of high frequencies in the elastic members, but also from the infinite frequencies associated with the kinematic constraints. Indeed, no mass is associated with the Lagrange multipliers giving rise to algebraic equations coupled to the other equations of the system which are differential in nature.

Two novel time integration schemes for flexible, nonlinear multi-body systems were developed by the first author [1, 2]. The first is an energy-preserving scheme that combines two features: an energy preservation statement for the elastic bodies and the vanishing of the work done by the forces of constraint. This results in exact preservation of the total energy for the nonlinear multi-body system and *unconditional stability* is achieved. The scheme exhibits second-order accuracy and has no numerical dissipation. The second scheme is an energy-decaying scheme that combines two features: an energy decay inequality for the elastic bodies and the vanishing of the work done by the forces of constraint. This results in the decay of the total energy of the multi-body system and *unconditional stability* is achieved. This scheme possesses third-order accuracy and high-frequency numerical dissipation.

Typical beam analysis used in multibody formulations rarely account for such basic effects as the shear center being offset from the sectional center of mass. The analysis of beam-like structures made of laminated composite materials requires a much more complicated methodology. Because of this complexity, it is common to find treatments of simple cross-sectional shapes (strips, box-beams, I-beams, etc.) as pointed out in a review article by the second author [3]. Although such analysis may be helpful in providing insight into the behavior of composite beams, they are essentially useless in the analysis of realistic composite beams used in engineering applications. In work of Berdichevsky [4], the three-dimensional elasticity representation of a beam was shown to give rise to two separate problems: a linear two-dimensional problem over the beam cross-section, which provides a set of elastic constants and a set of "recovering relations" for three-dimensional displacements, strain, and stress; and a nonlinear one-dimensional problem along the beam reference line.

An extension of this methodology to generally anisotropic and inhomogeneous beams was undertaken by Cesnik and Hodges [5]. The two-dimensional problem is solved by the finite element method, resulting in maximum generality. Results from application of this approach are very similar to those obtained from application of the pioneering work of [6]. The splitting of the three-dimensional problem into two- and one-dimensional parts results in a tremendous savings of computational effort relative to the cost of three-dimensional finite element analysis, the only alternative for realistic beams. The one-dimensional equations that fall out from this approach are the canonical intrinsic equations of motion for beams, as developed by many investigators; for example, see [7, 3, 8].

For the analysis of arbitrary beams (excluding those with thin-walled, open cross-sections) made of laminated, composite materials, a fully populated 4×4 matrix of elastic constants is found using the analysis of [5]. A refined model including transverse shear deformation is only necessary for beams which are either not slender or when high-frequency short-wavelength phenomena are investigated. The results obtained in this paper are based on the 4×4 model

and have been verified to be essentially identical to those obtained from a 6×6 matrix of elastic constants obtained from the analysis of [6].

The goal of this paper is to present an analysis methodology for nonlinear, flexible multibody dynamics systems involving elastic components made of laminated, anisotropic composite materials. The paper is organized in the following manner. Section 2 presents the kinematic notations and conventions used in this work. Section 3.1 develops the governing equations for beams undergoing arbitrarily large displacements and rotations but small strain. Section 3.2 describes a finite element based methodology for the evaluation of the sectional properties of beams made of composite materials, and a specific example is presented in section 4. Two numerical examples are presented in section 5.

2 Kinematic notations and conventions

The kinematic description of bodies and joints in their undeformed and deformed configurations will make use of three orthogonal triads. First, an inertial triad is used as a global reference for the system; it is denoted $\mathcal{S}_I$ with unit vectors $\vec{i}_1$, $\vec{i}_2$, and $\vec{i}_3$. A second triad $\mathcal{S}_0$, with unit vectors $\vec{e}_{01}$, $\vec{e}_{02}$, and $\vec{e}_{03}$ is attached to the body and defines its orientation in the reference configuration. Finally, a third triad $\mathcal{S}^*$ with unit vectors $\vec{e}_1$, $\vec{e}_2$, and $\vec{e}_3$ defines the orientation of the body in its deformed configuration.

Let $\vec{u}_0$ and $\vec{u}$ be the displacement vectors from $\mathcal{S}_I$ to $\mathcal{S}_0$, and $\mathcal{S}_0$ to $\mathcal{S}^*$, respectively, and $\mathbf{R}_0$ and $\mathbf{R}$ the rotation tensors from $\mathcal{S}_I$ to $\mathcal{S}_0$, and $\mathcal{S}_0$ to $\mathcal{S}^*$, respectively. In this work, all vector and tensor components are measured in either $\mathcal{S}_I$ or $\mathcal{S}^*$. For instance, the components of vector $\vec{u}$ measured in $\mathcal{S}_I$ and $\mathcal{S}^*$ will be denoted $\underline{u}$ and $\underline{u}^*$, respectively, and clearly

$$\underline{u}^* = R_0^T R^T \ \underline{u}. \tag{1}$$

The superscript $(.)^*$ will be used to denote tensor components measure in $\mathcal{S}^*$. Similarly, the components of tensor $\mathbf{R}$ measured in $\mathcal{S}_I$ and will be denoted by R. For brevity sake, a compact notation will be used to deal with the components of the linear and angular vectors simultaneously. For instance,

$$\underline{v} = \left\{ \begin{array}{c} \hat{\underline{v}} \\ \check{\underline{v}} \end{array} \right\} \tag{2}$$

defines the six components of the velocity vector consisting of the three components linear and angular velocities denoted $\hat{\underline{v}}$ and $\check{\underline{v}}$, respectively. The following 6×6 operators are introduced

$$\mathcal{R}_0 = \left[\begin{array}{cc} R_0 & 0 \\ 0 & R_0 \end{array} \right]; \quad \mathcal{R} = \left[\begin{array}{cc} R & 0 \\ 0 & R \end{array} \right]; \quad \mathcal{U}\left[.\right] = \left[\begin{array}{cc} 0 & 0 \\ [.] & 0 \end{array} \right]. \tag{3}$$

The skew-symmetric matrix formed with the components $\underline{u}$ will be denoted $\widetilde{u}$.

3 Formulation of beam elements made of anisotropic materials

The three-dimensional elasticity representation of a beam was shown [4] to give rise to two separate problems, as depicted in a symbolic manner in fig. 1. The first problem is a

linear, two-dimensional problem over the beam cross-section to be discussed in more detail in section 3.2. This analysis provides a set of elastic constants characterizing the beam cross-section and a set of "recovery relations" relating the three-dimensional displacements, strain, and stress fields in the beam to generalized one-dimensional strain measures. The second problem is a nonlinear, one-dimensional problem along the beam reference line to be discussed in more detail in section 3.1. This analysis predicts the nonlinear response of the beam when subjected to time dependent loads.

These two analysis work together to provide a methodology for the simulation of multibody systems involving beams made of anisotropic materials. At first, the sectional properties of the beam are computed based on a linear, two-dimensional finite element analysis of the beam cross-section. These properties are used to define the physical characteristics of the beams involved in the multibody system. Next, the dynamic response of the multibody system is computed using a nonlinear, finite element procedure. At the post-processing state, the predicted generalized strain measures are used in conjunction with the recovery relations to evaluate the beam three-dimensional displacement, stress, and strain distributions.

3.1 Beam analysis

Beams can be defined as elastic bodies whose volume is that spanned by a cross-section translating along a smooth reference line. The cross-section lies in the plane defined by vectors $\vec{e}_{02}$, $\vec{e}_{03}$ and $\vec{e}_2$, $\vec{e}_3$ in the undeformed and deformed configurations, respectively, as depicted in fig. 2. The kinetic and strain energies of the beam are

$$\mathcal{K} = \frac{1}{2}\int_0^L \underline{v}^{*T} M^* \underline{v}^* \, dx_1; \quad \mathcal{V} = \frac{1}{2}\int_0^L \underline{e}^{*T} C^* \underline{e}^* \, dx_1, \tag{4}$$

respectively. L is the length of the beam; x_1 the curvilinear coordinate along the reference line; M^* and C^* the components of the sectional inertial and stiffness tensor, respectively; and $\underline{v}^*$, and $\underline{e}^*$ the components of the sectional velocity and strain vectors, respectively. The 6×6 inertial matrix M^* is fully populated, allowing the modeling of rotary inertia effects and the offset of the sectional mass center with respect to the reference line. Similarly, the 6×6 stiffness matrix C^* is fully populated, allowing the modeling of shearing deformation effect, the offset of tension center and shear center with respect to the reference line, and all elastic couplings that might arise from the use of tailored composite materials. The velocity-displacement and strain-displacement relationships are

$$\underline{v} = \left\{ \begin{array}{c} \hat{\underline{v}} \\ \check{\underline{v}} \end{array} \right\} = \left\{ \begin{array}{c} \dot{\underline{u}} \\ \check{\underline{v}} \end{array} \right\}; \quad \underline{e} = \left\{ \begin{array}{c} \hat{\underline{e}} \\ \check{\underline{e}} \end{array} \right\} = \left\{ \begin{array}{c} (\underline{u}_0' + \underline{u}') - RR_0 \, \underline{\imath}_1 \\ \check{\underline{e}} \end{array} \right\}, \tag{5}$$

where $(.)^{\cdot}$ and $(.)'$ denote derivatives with respect to time and x_1, respectively; $\check{\underline{v}}$ are the components of the sectional angular velocity vector, with $\widetilde{\check{v}} = \dot{R}\, R^T$; and $\check{\underline{e}}$ the components of the sectional elastic curvature vector, with $\widetilde{\check{e}} = R' R^T$. These relationships are geometrically exact, *i.e.* are valid for arbitrarily large displacements and rotations, although the strain is assumed to remain small. Virtual variations in sectional velocities and strains are

$$\delta \underline{v}^{*T} = \left(\underline{\delta \dot{d}}^T - \underline{\delta d}^T \, \mathcal{U}[\widetilde{\check{u}}] \right) \mathcal{R}\mathcal{R}_0; \tag{6}$$

$$\delta \underline{e}^{*T} = \left(\underline{\delta d}'^T - \underline{\delta d}^T \, \mathcal{U}[\widetilde{u}_0' + \widetilde{u}'] \right) \mathcal{R}\mathcal{R}_0, \tag{7}$$

where $\underline{\delta d}^T = (\delta \underline{u}^T, \ \underline{\delta \psi}^T)$ are the virtual displacements and rotations. The virtual rotations are defined as $\widetilde{\delta \psi} = \delta R \ R^T$.

The equations of motion of the beam will be derived from Hamilton's principle

$$\int_{t_i}^{t_f} \int_0^L \left(\delta \underline{v}^{*T} M^* \underline{v}^* - \delta \underline{e}^{*T} C^* \underline{e}^{*T} + \delta \mathcal{W}^a \right) dx_1 \ dt = 0, \tag{8}$$

where $\delta \mathcal{W}^a$ is the virtual work done by the externally applied forces. The equations of motion of the beam are found by introducing eqs. (6) and (7), and using the strain and velocity expressions, eqs. (5), to find

$$\left(\mathcal{R}\mathcal{R}_0 \ \underline{p}^* \right)^{\cdot} + \mathcal{U}[\widetilde{\dot{u}}] \ \mathcal{R}\mathcal{R}_0 \ \underline{p}^* - \left(\mathcal{R}\mathcal{R}_0 \ \underline{f}^* \right)' - \mathcal{U}[\widetilde{u}_0' + \widetilde{u}'] \ \mathcal{R}\mathcal{R}_0 \ \underline{f}^* = \underline{q}; \tag{9}$$

where the sectional momenta and elastic forces are defined as $\underline{p}^* = M^* \ \underline{v}^*$ and $\underline{f}^* = C^* \ \underline{e}^*$, respectively; and $\underline{q}$ are the external forces.

These equations can be discretized in such a manner that they imply a discrete energy preservation or decay statement, leading to the unconditional stability of the resulting time integration scheme. Details of this procedure can be found in [1] and will not be repeated here. Constraint forces can be readily treated within this framework: they can be discretized in such a manner that the work they perform vanishes exactly. The combination of these two features leads to unconditionally stable schemes for flexible, nonlinear constrained multibody systems.

3.2 Beam cross-sectional analysis

The purpose of the beam cross-sectional analysis is to determine the elements of the matrix C^* and the recovering relations. The cross-sectional stiffness matrix C^* relates the cross-sectional stress resultants $\underline{f}^*$ to the generalized strain measures $\underline{e}^*$ [5], a 1-D constitutive law. Recovering relations provide the relationship between the strain tensor components and the generalized strain measures $\underline{e}^*$ [9]. (Alternatively, some researchers have developed recovering relations for the stress tensor components in terms of the cross-sectional stress resultants $\underline{f}^*$ [6].)

In the present notation, the 1-D constitutive law can be written as

$$\underline{f}^* = C^* \underline{e}^* \tag{10}$$

where $\underline{f}^* = \lfloor f_1 \ f_2 \ f_3 \ m_1 \ m_2 \ m_3 \rfloor^T$ with f_1 as the axial force, f_2 and f_3 as transverse shear forces, m_1 as the twisting moment, m_2 and m_3 as the bending moments; $\underline{e}^* = \lfloor \hat{e}_{11} \ \hat{e}_{12} \ \hat{e}_{13} \ \check{e}_1 \ \check{e}_2 \ \check{e}_3 \rfloor^T$ with $\hat{e}_{11}$ as the axial stretching measure of the beam, $\hat{e}_{12}$ and $\hat{e}_{13}$ as transverse shear measures, $\check{e}_1$ as the elastic twist per unit length, and $\check{e}_2$ and $\check{e}_3$ as elastic components of the curvature.

Ref. [5] develops various levels of cross-sectional analysis by use of asymptotic methods. The simplest approximation provides a 4×4 matrix of cross-sectional stiffnesses, with infinite stiffness associated with the transverse shear measures, the second and third rows and

columns of C^*. This approximation is adequate as long as the ratio of the wavelength of the deformation to the characteristic diameter of the cross section remains large compared to unity. Typical cases for which this ratio is not sufficiently large include fat beams, thin-walled open sections, and high-frequency phenomena. In such cases, the transverse shear stiffnesses may need to be determined, and possibly other non-classical cross-sectional motion needs to be taken into account as well. For the present problem we have verified that the 4×4 matrix is adequate. This matrix accounts for extension, twist, and two bending measures.

The diagonal terms of this matrix are present for all beams, but it is possible to choose the cross-sectional coordinate system for prismatic, isotropic beams so that the off-diagonal terms are zero. However, for anisotropic beams, the matrix is fully populated in general, so that extension-twist coupling, bending-twist coupling, and bending-bending coupling can be accounted for. Initial twist and curvature can affect all the elements of the matrix [10].

The computer code VABS [5] accounts for all possible deformations in the 3-D elastic model. Although the example configurations treated herein are thin-walled box-beams, the code is capable of treating built-up structures of arbitrary complexity. There are no restrictions on the cross-sectional geometry or materials that can be modeled with VABS, and the effects of initial twist and curvature can be treated as well.

4 Analysis of a thin-walled rectangular section

To illustrate the cross-sectional analysis process described in the previous section, the sectional properties the thin-walled, rectangular section depicted in fig. 3 will be presented here. The section is 0.953×0.537 *in* and was the object of experimental, numerical and analytical studies carried out by Chopra [11, 12] and later by Borri [13]. The walls consist of six, 0.005 *in* thick plies of graphite/epoxy material with the following material properties: longitudinal modulus $E_L = 20.59 \times 10^6$ *psi*, transverse modulus $E_T = 1.42 \times 10^6$ *psi*, shearing modulus $G_{LT} = 0.87 \times 10^6$ *psi*, and Poisson's ratio $\nu_{LT} = 0.42$. Three different lay-ups, described in Table 1, were considered here. Lay-up definitions start with the innermost ply (*ply 1*) and end with the outermost ply (*ply 6*); 0° fibers are aligned with the axis of the beam and a positive ply angle indicates a right-hand rotation about the local normal to the thin wall.

The various sections were analyzed using the finite element procedure outlined in section 3.2. The mesh consisted of 288 eight-noded quadrilateral elements for a total of 2880 degrees of freedom. The sectional properties for *lay-up 1* were found to be

$$C_1^* = 10^{+3} \begin{bmatrix} 1770 & 0.00 & 0.00 & 0.00 & 0.00 & 0.00 \\ & 1770 & 0.00 & 0.00 & 0.00 & 0.00 \\ & & 1770 & 0.00 & 0.00 & 0.00 \\ & & & 8.16 & 0.00 & 0.00 \\ & & & & 86.9 & 0.00 \\ & & & & & 215 \end{bmatrix}. \tag{11}$$

This lay-up presents no elastic couplings and will be used as a reference. The 4×4 stiffness matrix obtained from the finite element analysis of section 3.2 was augmented with two row

and columns corresponding to the shear forces. The shearing stiffnesses were selected to be large numbers, equal to the axial stiffness. The sectional properties of *lay-up 2* were

$$C_2^* = 10^{+3} \begin{bmatrix} 1250 & 0.00 & 0.00 & 52.1 & 0.00 & 0.00 \\ & 1250 & 0.00 & 0.00 & 0.00 & 0.00 \\ & & 1250 & 0.00 & 0.00 & 0.00 \\ & & & 17.7 & 0.00 & 0.00 \\ & & & & 61.4 & 0.00 \\ & & & & & 1520 \end{bmatrix}. \tag{12}$$

Note the presence of an extension-twist coupling term for this lay-up. Finally, the sectional properties of *lay-up 3* were

$$C_3^* = 10^{+3} \begin{bmatrix} 1370 & 0.00 & 0.00 & 0.00 & 0.00 & 0.00 \\ & 1370 & 0.00 & 0.00 & 0.00 & 0.00 \\ & & 1370 & 0.00 & 0.00 & 0.00 \\ & & & 17.3 & 18.0 & 0.358 \\ & & & & 60.8 & 0.377 \\ & & & & & 143.0 \end{bmatrix}. \tag{13}$$

Note the presence of a non-negligible bending-twist coupling term for this lay-up (along with other very small bending-twist coupling in the other direction and very small bending-bending coupling). For all three lay-ups the mass matrix was

$$M^* = 10^{-6} \begin{bmatrix} 16.1 & 0.00 & 0.00 & 0.00 & 0.00 & 0.00 \\ & 16.1 & 0.00 & 0.00 & 0.00 & 0.00 \\ & & 16.1 & 0.00 & 0.00 & 0.00 \\ & & & 2.74 & 0.00 & 0.00 \\ & & & & 0.79 & 0.00 \\ & & & & & 1.95 \end{bmatrix}. \tag{14}$$

5 Numerical Examples

The examples presented in this section were integrated using the energy decaying scheme discussed in [1].

5.1 The actuated beam problem

The first example deals with the actuated beam problem depicted in fig. 4. A cantilevered beam of length $L = 100\ in$ with a tip mass $M_T = 0.02\ slug$ is actuated at its mid-point M by a crank and link mechanism. The crank of length $L_c = 8\ in$ is connected to the ground at point A and to a link of length $L_l = 8 \times \sqrt{2}\ m$ at point B. The link is connected to the beam at point M. Connections at points A and B use revolute joints, whereas the connection at point M is by means of a spherical joint. A torque is applied to the at point A so as to enforce a constant angular velocity for the crank $\Omega = \pi\ rad/sec$. The crank is a rigid body with a mass moment of inertia $I_c = 2.2 \times 10^{-5}\ slug.in^2$. The beam and link were modeled with eight and two cubic beam elements, respectively.

The response of the system will be presented for three complete cycles of the crank. Fig. 5 shows the tip displacements of the beam. Elastic vibrations are superposed onto the overall motion imparted by the crank and similar motions are observed for the three lay-ups. Note the very large transverse deflection of the beam, of up to 30 *in*, *i.e.* 30% of its length. For *lay-up 1*, the motion of the beam is purely two-dimensional, whereas for *lay-ups 2* and *3* three-dimensional motion is induced by the extension-twist and bending-twist couplings, respectively. This fact is illustrated in fig. 6 which shows the out-of-plane displacement of the beam tip. Although modest displacements of about 1.8 *in* only are observed for *lay-up 2*, displacements of up to 10 *in* occur for *lay-up 3*.

Under the effect of the crank actuation, large bending moments develop at the root of the beam, as depicted in fig. 7. The significantly higher bending moment observed for *lay-up 1* stems from the higher sectional stiffness of this lay-up featuring 0° plies only. *Lay-ups 2* and *3* also develop out-of-plane bending and twisting moments shown in figs. 8 and 9, respectively.

In a laminated composite structure, the local stress distribution is far more complex than for homogeneous, isotropic constructions. Fig. 10 shows the distribution of axial stress at the root of the beam, through the thickness of the section wall at location E (see fig. 3), at time $t = 1.5$ *sec*. The axial stress distribution is nearly uniform through the thickness for *lay-ups 1* and *3* as should be expected since all plies have the same fiber orientation. For *lay-up 2*, axial stresses differ by a factor of about 4 in the 0° plies as compared to the 30° plies. Similarly, fig. 11 shows the distribution of shear stress at the same location. Note that for *lay-up 2* and *lay-up 3* shear stresses are two and eight times larger than those of *lay-up 1*, respectively.

Finally, figs. 12 and 13 show the time history of the axial and shear stresses, respectively. The root stresses are plotted at location E, at the mid-point of *plies 1* and *2*. The much larger shear stresses in *lay-ups 2* and *3* are present at nearly all times. Fig. 14 shows the corresponding root axial stresses at location D (see fig. 3). The much larger axial stresses in *lay-up 3* stem from the significant out-of-plane bending moment present in this case, see fig. 8.

5.2 The suspension problem

The second numerical example deals with the simplified model of a vehicle rear suspension, depicted in fig. 15. A 20 *in* long elastic arm is attached to the vehicle chassis at point R by means of a revolute joint allowing rotation about axis $\vec{\imath}_1$. A torsional spring with a stiffness constant $k_\theta = 10^{+3}$ *lb.in/rad* and a torsional damper with a damping constant $\mu_\theta = 5$ *lb.in/rad/sec* are present at the revolute joint. At point A, the arm connects to a 3 *in* long elastic wheel support to which the wheel is attached at point W. The arm and wheel support are modeled with four and two cubic beam elements, respectively. The suspension is subjected to a time dependent, vertical force $F(t)$ applied at point W with the following history

$$F(t) = \begin{cases} 5(1-\cos 2t) + (1-\cos 10t) & t \leq 0.5 \ sec \\ 0 & t > 0.5 \ sec. \end{cases}$$

The wheel support consists of a thin-walled beam with the cross-section described in section 4 using *lay-up 1*. Two different cases will be contrasted corresponding to the choice of *lay-ups*

1 and *3* for the elastic arm.

As the load $F(t)$ is applied to the wheel, both bending and twisting moments develop in the arm. The bending moment causes rotation of the revolute joint at R, and vertical elastic displacements of the arm. The twisting moment creates an elastic rotation of the arm about axis $\vec{e}_1$, which in turns, rotates the wheel about the same axis. It is, however, desirable for the wheel to remain normal to the road and this is generally achieved through kinematic means by a number of articulated linkages. In this example, it will be shown that the same effect can be achieved through proper elastic tailoring of the arm. Let moments M_1, M_2, and M_3 be positive about axes $\vec{e}_1$, $\vec{e}_2$, and $\vec{e}_3$, respectively. A similar convention is used for the forces F_1, F_2, and F_3 along the same axes. On the other hand, the displacements u_1, u_2, and u_3 are positive along axes $\vec{i}_1$, $\vec{i}_2$, and $\vec{i}_3$, respectively. Rotations ϕ_1, ϕ_2, and ϕ_3 are positive about the same axes. For *lay-up 3*, the bending-twisting coupling term is such that the bending moment M_2 created by the applied load induces a positive twist ϕ_2 that nearly cancels out the negative twist associated with the torsion of the arm under the applied load. Consequently, the wheel remains nearly normal to the road as it deflects upward under the effect of the applied load. The configuration of the elastically tailored suspension is far simpler than that required to achieve such effect through more conventional kinematic means.

Fig. 16 shows that the time history of the vertical displacements of the wheel at point W are nearly identical for the two lay-ups, reaching a maximum deflection of about 6 *in*. The wheel lateral deflection u_1 at the same point is shown in fig. 17: the maximum deflection of 0.025 *in* observed for *lay-up 1* is reduced tenfold to about 0.0025 *in* for *lay-up 3*. The rotation ϕ_1 and ϕ_2 of the wheel are depicted in figs. 18 and 19, respectively. Rotations ϕ_1 were nearly identical for the two lay-ups, as expected since nearly identical vertical deflections were observed. On the other hand, the 0.1 *rad* ϕ_2 rotation obtained with *lay-up 1* is reduced 25 times to about 0.004 *rad* for *lay-up 3*. Clearly, the proposed elastic tailoring of the suspension arm considerably reduces both side slipping and tilting of the wheel with respect to the road, while maintaining the other characteristics of the suspension nearly unchanged.

Next, the stress resultants at the root of the arm will be presented. Figs. 20, 21, and 22 show the root shear force F_3, twisting moment M_1, and bending moment M_2, respectively. These stress resultants are nearly identical for the two lay-up. However, in laminated composite structures, nearly identical stress resultant do not imply nearly identical local stress levels. Figs. 23 and 24 show the axial and shear stress distributions through the thickness of the wall, respectively, at locations D and E. At location E, *lay-up 3* axial stresses are up to three times those for *lay-up 1*, and shear stresses are about 50% higher. In contrast, stress level are nearly identical at location D.

The time history of the axial and shearing stresses at the mid-point of *plies 1* and *2* are depicted in figs. 25 and 26 for location D, and in figs. 27 and 28 for location E. Similar time histories are observed at location D, whereas large differences in stress levels are apparent at location E throughout the time history.

6 Conclusions

This paper has described an methodology for the dynamic analysis of flexible, nonlinear multi-body systems involving elastic members made of laminated, anisotropic composite materials. The analysis methodology consists of a three step procedure. First, the sectional properties of beams made of composite materials are determined based on an asymptotic procedure that involves a two-dimensional finite element analysis of the cross-section. Second, the dynamic response of nonlinear, flexible multi-body systems is simulated within the framework of energy-preserving and energy-decaying time integration schemes that provide unconditional stability for nonlinear systems. Finally, local three-dimensional stresses in the beams are recovered, based on the stress resultants predicted in the previous step.

Numerical examples were presented that demonstrate the profound effect elastic couplings can have on the dynamic response of multi-body systems made of laminated, anisotropic composite materials. These elastic coupling can be used to tailor the dynamic response of the system to obtain desirable features. The simplified model of a vehicle rear suspension was presented. The suspension features an elastically tailored arm which was shown to considerably reduce both side slipping and tilting of the wheel with respect to the road, while maintaining the other characteristics of the suspension nearly unchanged. The configuration of the elastically tailored suspension is far simpler than that required to achieve such effect through more conventional kinematic means.

References

[1] O.A. Bauchau. Computational schemes for flexible, nonlinear multi-body systems. *Multibody System Dynamics*, 2:169–225, 1998.

[2] O.A. Bauchau and T. Joo. Computational schemes for nonlinear elasto-dynamics. *International Journal for Numerical Methods in Engineering*, 45:693–719, 1999.

[3] D.H. Hodges. A review of composite rotor blade modeling. *AIAA Journal*, 28(3):561–565, March 1990.

[4] V.L. Berdichevsky. On the energy of an elastic rod. *PMM*, 45:518–529, 1982.

[5] C.E.S. Cesnik and D.H. Hodges. VABS: a new concept for composite rotor blade cross-sectional modeling. *Journal of the American Helicopter Society*, 42(1):27–38, January 1997.

[6] V. Giavotto, M. Borri, P. Mantegazza, G. Ghiringhelli, V. Carmaschi, G.C. Maffioli, and F. Mussi. Anisotropic beam theory and applications. *Computers and Structures*, 16(1-4):403–413, 1983.

[7] M. Borri and T. Merlini. A large displacement formulation for anisotropic beam analysis. *Meccanica*, 21:30–37, 1986.

[8] O.A. Bauchau and N.K. Kang. A multi-body formulation for helicopter structural dynamic analysis. *Journal of the American Helicopter Society*, 38:3–14, 1993.

[9] C.E.S. Cesnik, D.H. Hodges, B. Popescu, and D. Harursampath. Composite beams cross-sectional modeling including obliqueness and trapeze effects. In *Proceedings of the 37th Structures, Structural Dynamics and Materials Conference*, pages 1384–1397, Salt Lake City, Utah, April 15-17, 1996. AIAA Paper 96-1469.

[10] C.E.S. Cesnik, D.H. Hodges, and V.G. Sutyrin. Cross-sectional analysis of composite beams including large initial twist and curvature effects. *AIAA Journal*, 34(9):1913–1920, Sept. 1996.

[11] R. Chandra, H. Ngo, and I. Chopra. Experimental study of thin-walled composite beams. In *Proceedings of the American Helicopter Society National Technical Specialists' Meeting on Advanced Rotorcraft Structures*, 1988.

[12] E.C. Smith and I. Chopra. Formulation and evaluation of an analytical model for composite box beams. In *Proceedings of the 31st AIAA/ AHS/ ASME/ ASCE/ ASC Structures, Structural Dynamics and Material Conference, Long Beach, California*, 1990.

[13] M. Borri, G.L. Ghiringhelli, and T. Merlini. Composite beam analysis: Linear analysis of naturally curved and twisted anisotropic beams. Technical report, Politecnico di Milano, 1992.

List of Tables

List of Figures

Lay-up type	Upper wall	Lower wall	Left wall	Right wall
Lay-up 1	$[0^\circ_6]$	$[0^\circ_6]$	$[0^\circ_6]$	$[0^\circ_6]$
Lay-up 2	$[(30^\circ, 0^\circ)_3]$	$[(30^\circ, 0^\circ)_3]$	$[(30^\circ, 0^\circ)_3]$	$[(30^\circ, 0^\circ)_3]$
Lay-up 3	$[15^\circ_6]$	$[-15^\circ_6]$	$[\mp 15^\circ_3]$	$[\pm 15^\circ_3]$

Table 1: Definition of the three lay-ups.

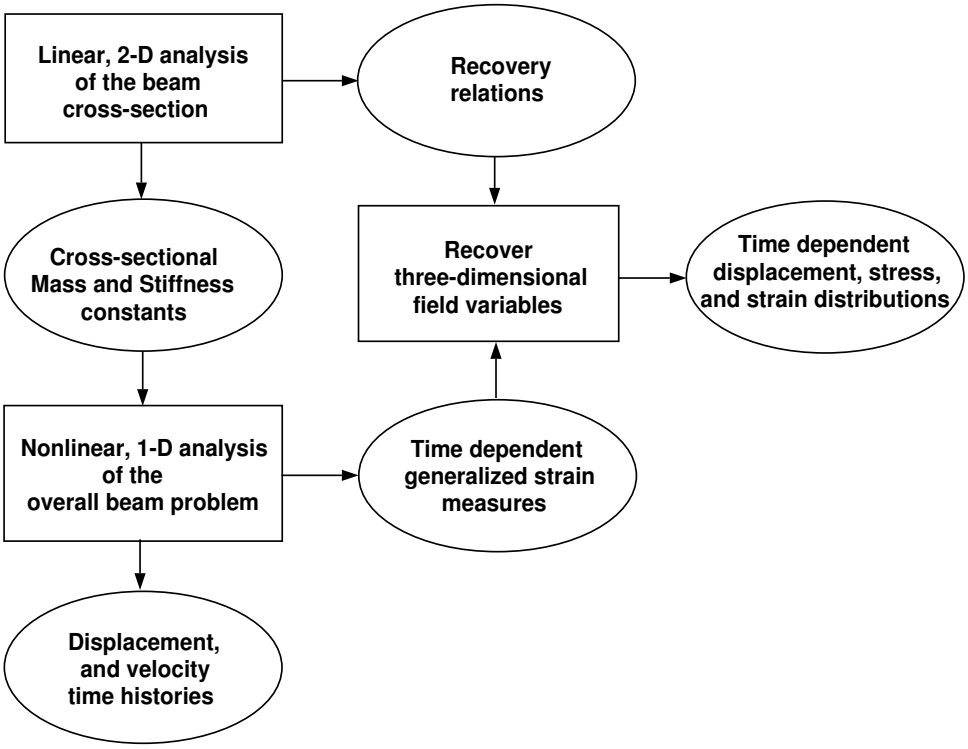

Figure 1: Analysis of a three-dimensional beam.

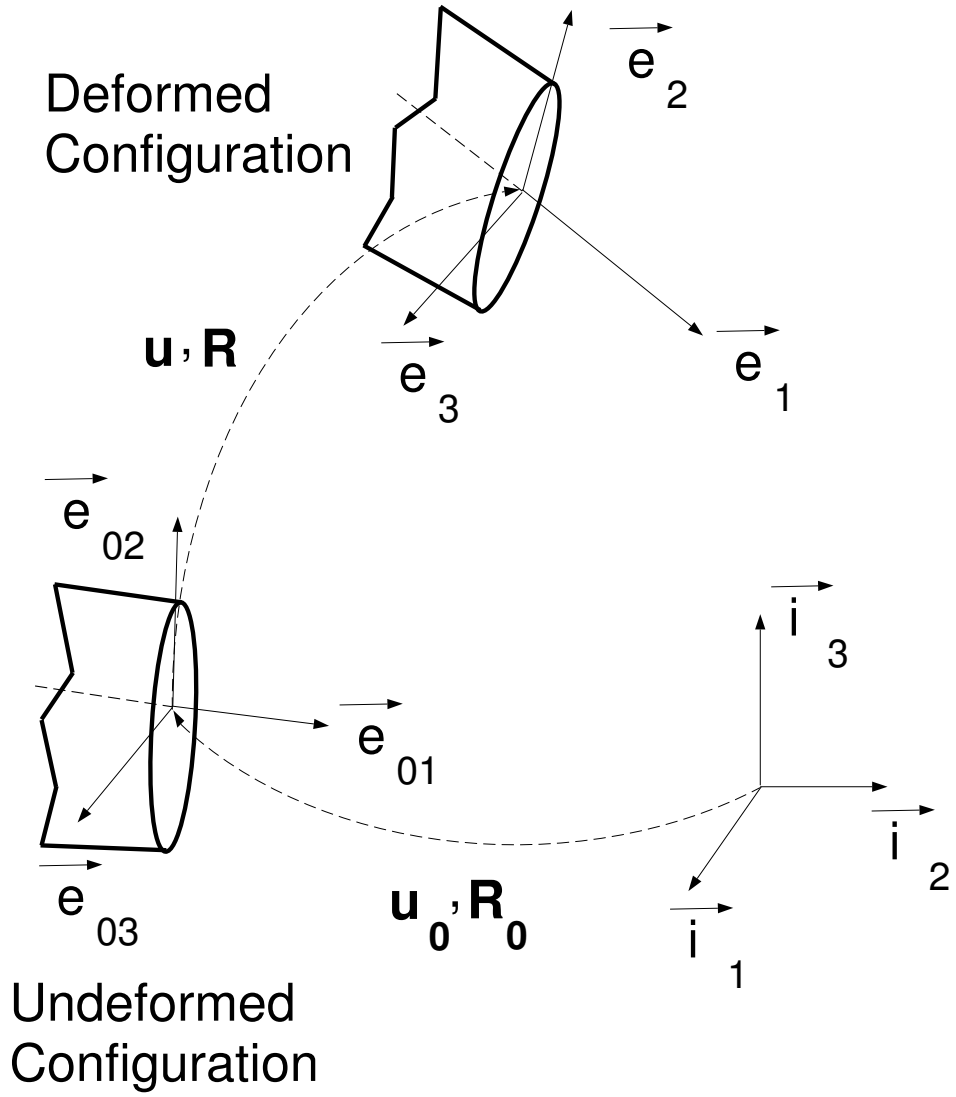

Figure 2: Beam in the undeformed and deformed configurations.

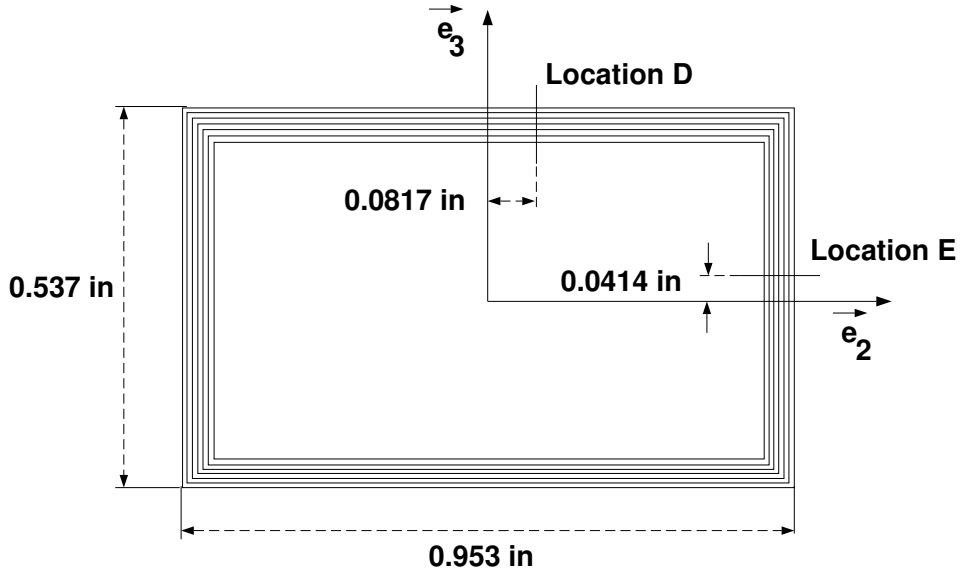

Figure 3: The thin-walled rectangular cross-section.

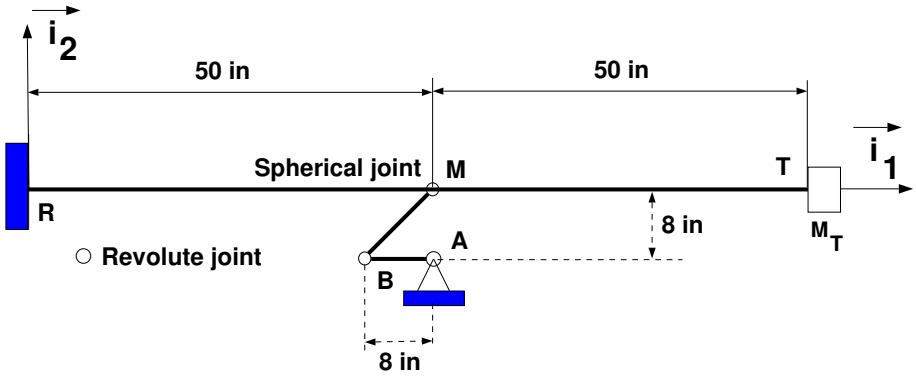

Figure 4: The actuated beam problem.

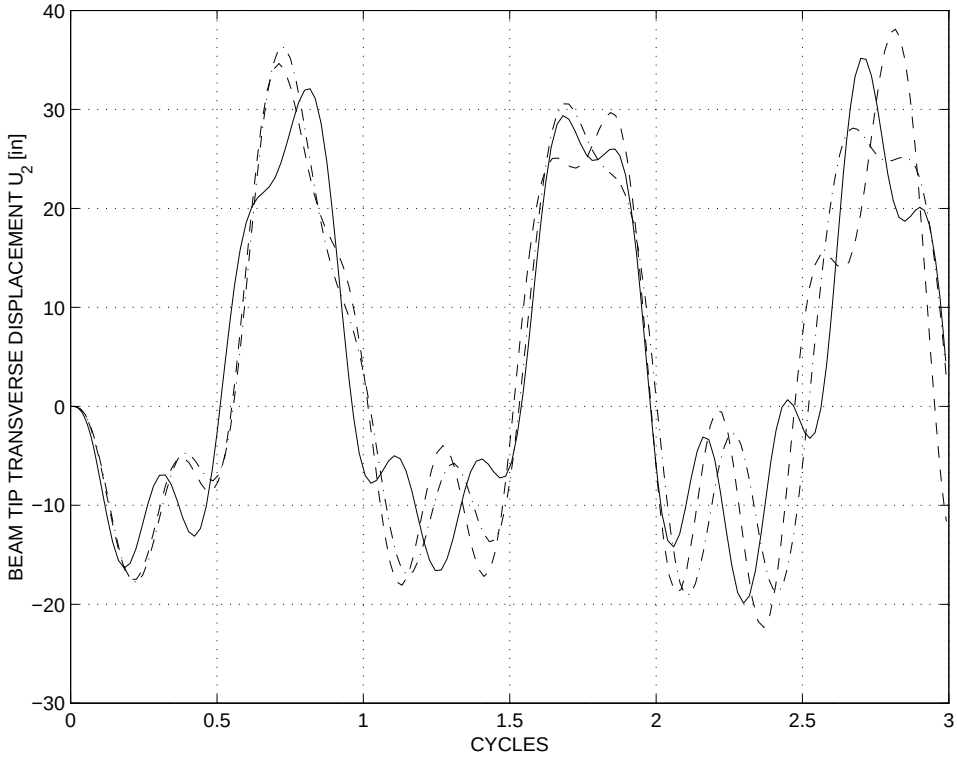

Figure 5: Tip transverse deflections u_2 of the beam. Solid line: *Lay-up 1*; dashed line: *Lay-up 2*; dashed-dot line: *Lay-up 3*.

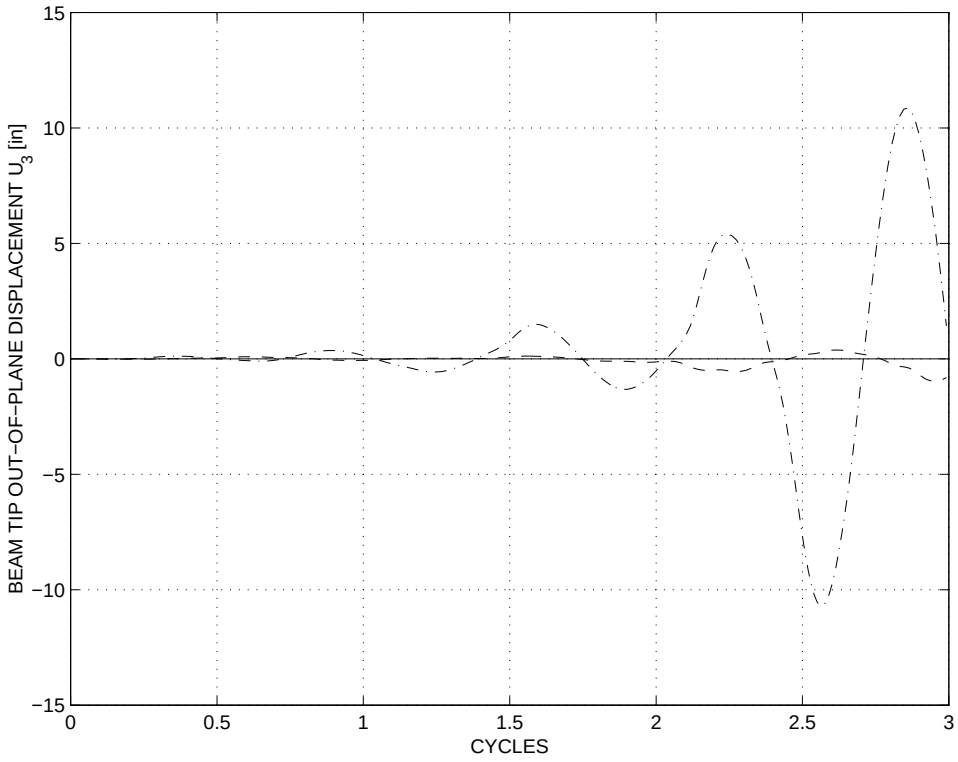

Figure 6: Tip out-of-plane deflections u_3 of the beam. *Lay-up 1*: solid line; *lay-up 2*: dashed line; *lay-up 3*: dashed-dot line.

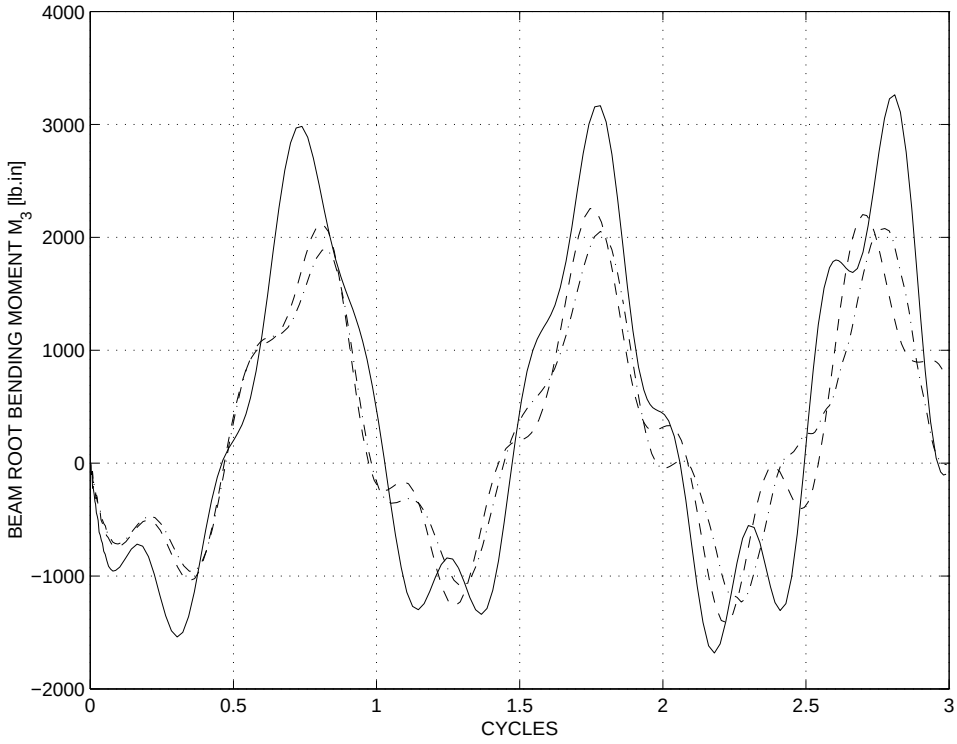

Figure 7: Beam root bending moments M_3. *Lay-up 1*: solid line; *lay-up 2*: dashed line; *lay-up 3*: dashed-dot line.

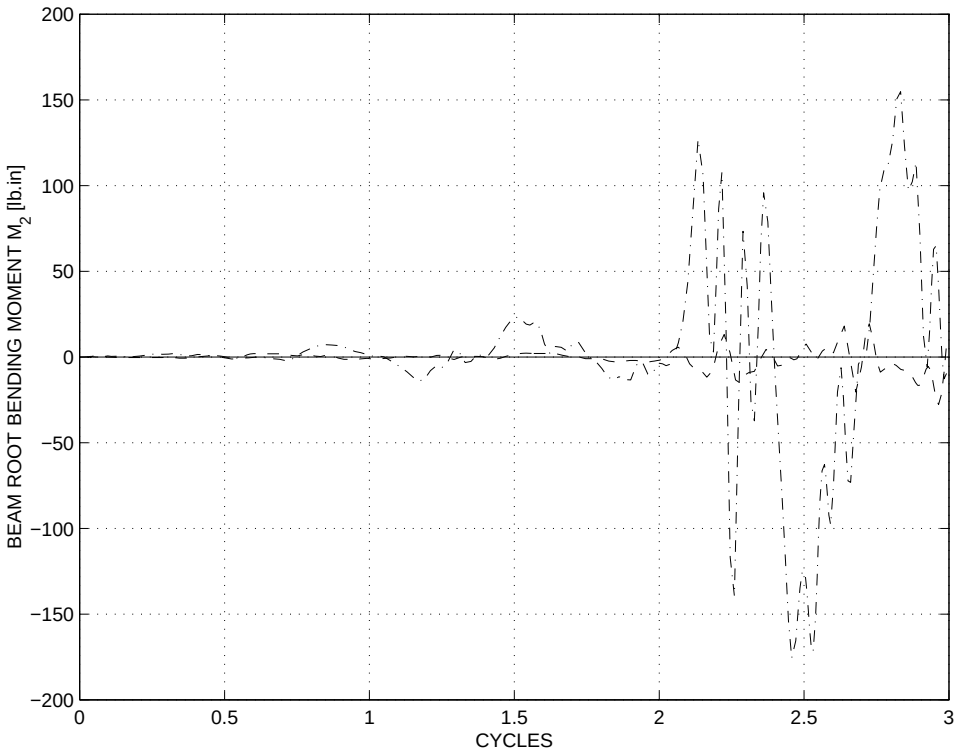

Figure 8: Beam root bending moments M_2. *Lay-up 1*: solid line; *lay-up 2*: dashed line; *lay-up 3*: dashed-dot line.

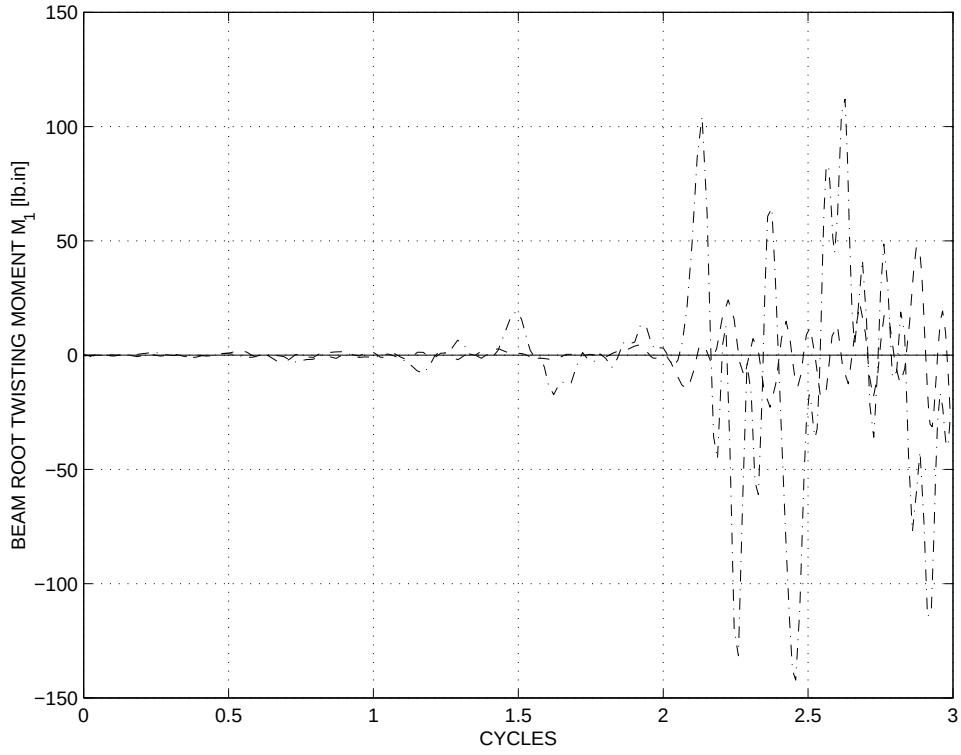

Figure 9: Beam root twisting moment M_1. *Lay-up 1*: solid line; *lay-up 2*: dashed line; *lay-up 3*: dashed-dot line.

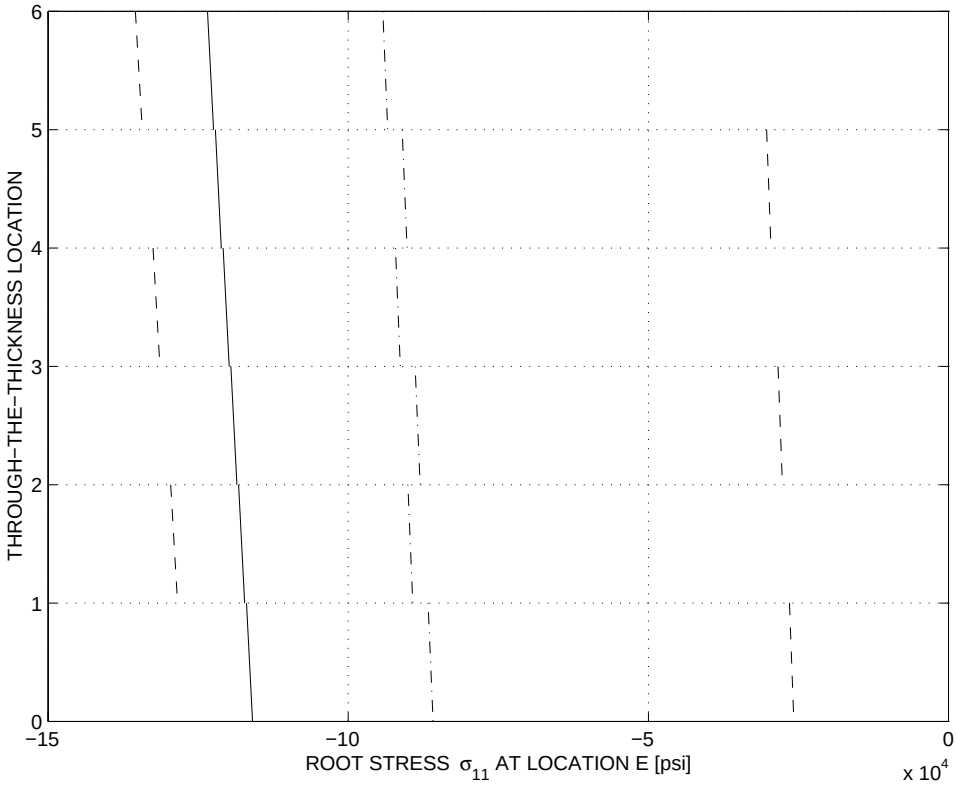

Figure 10: Distribution of beam root axial stress σ_{11} through the thickness of the laminate at location E. *Lay-up 1*: solid line; *lay-up 2*: dashed line; *lay-up 3*: dashed-dot line.

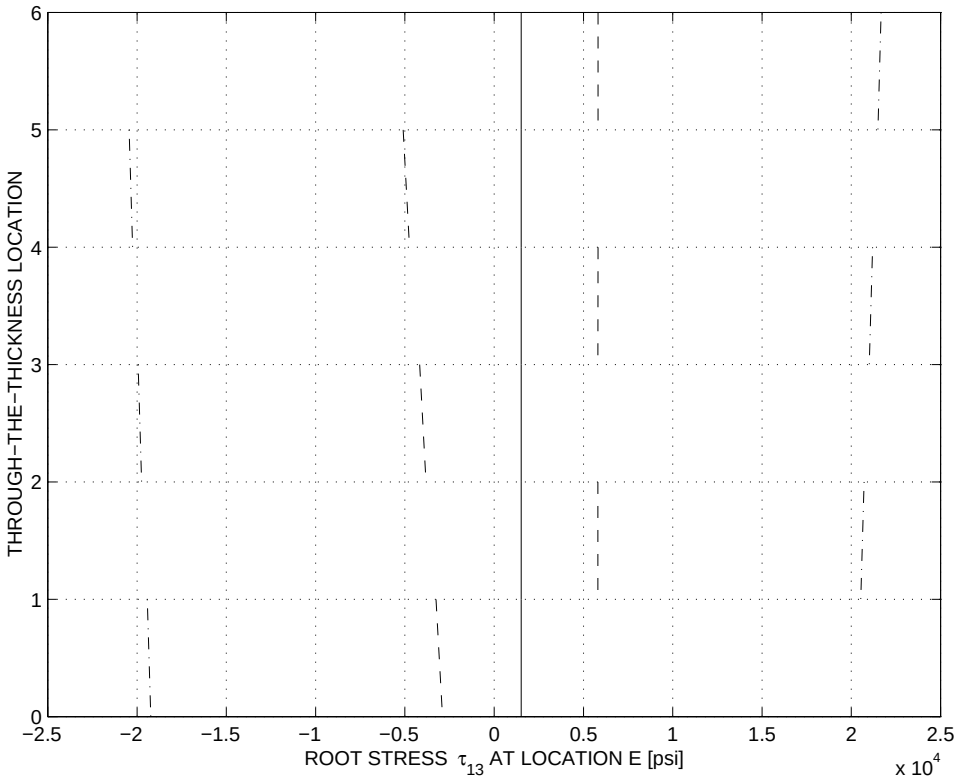

Figure 11: Distribution of beam root shear stress τ_{13} through the thickness of the laminate at location E. *Lay-up 1*: solid line; *lay-up 2*: dashed line; *lay-up 3*: dashed-dot line.

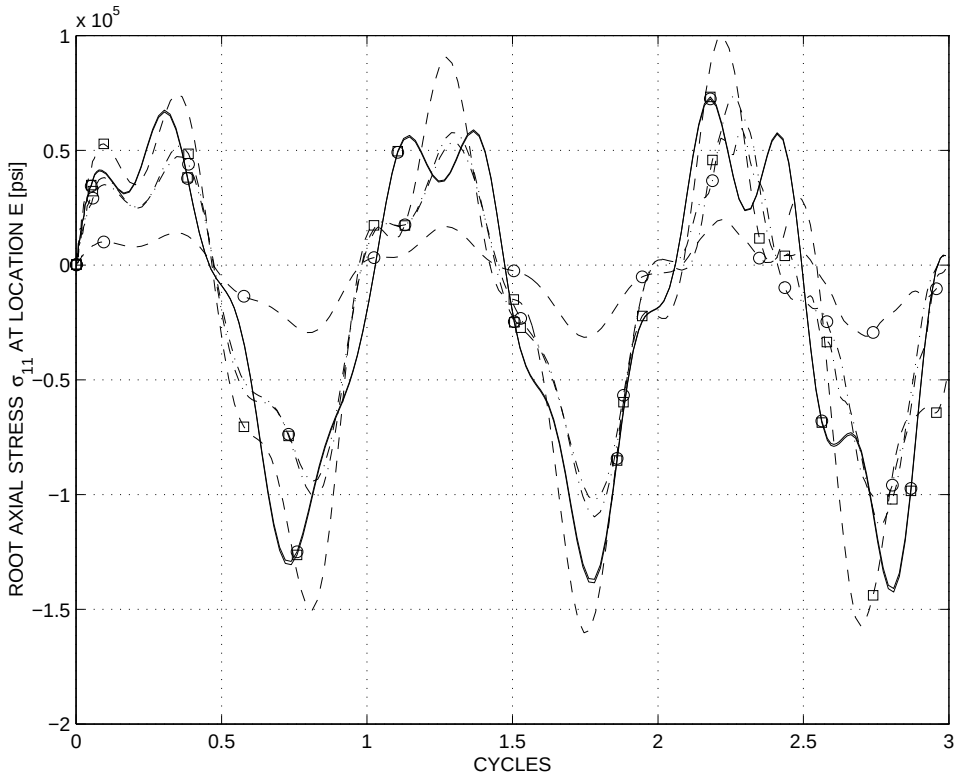

Figure 12: Time history of the beam root axial stress σ_{11} at location E. *Lay-up 1*: solid line; *lay-up 2*: dashed line; *lay-up 3*: dashed-dot line. *Ply 1* stresses: ($\circ$); *ply 2* stresses: ($\square$).

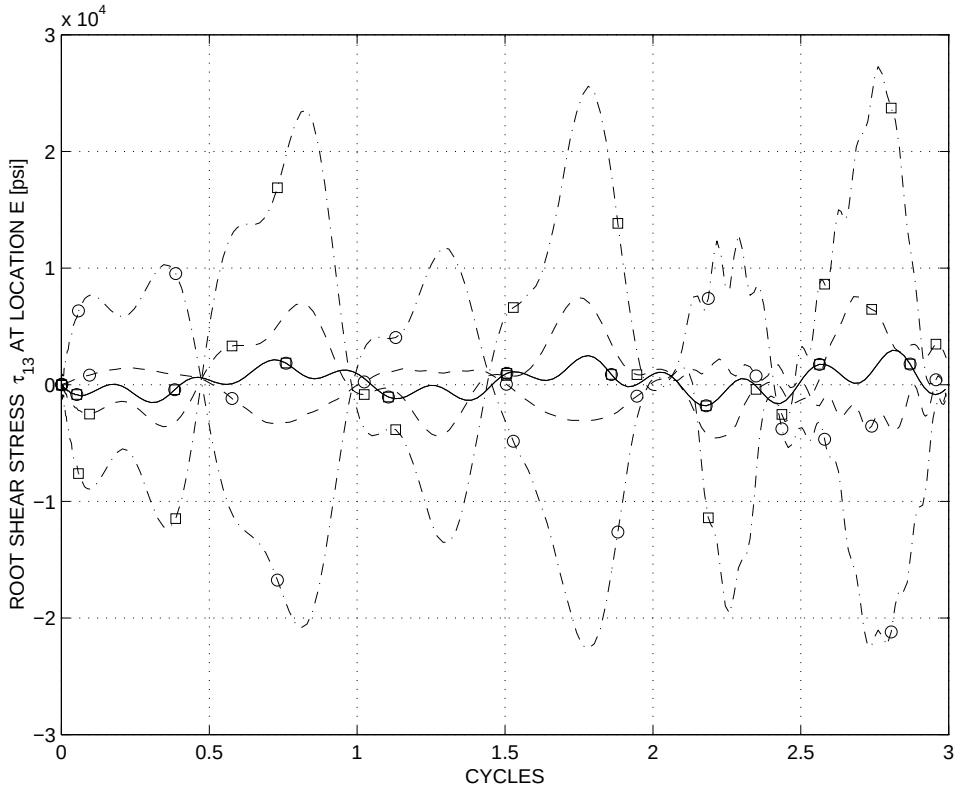

Figure 13: Time history of the beam root shear stress τ_{13} at location E. *Lay-up 1*: solid line; *lay-up 2*: dashed line; *lay-up 3*: dashed-dot line. *Ply 1* stresses: ($\circ$); *ply 2* stresses: ($\square$).

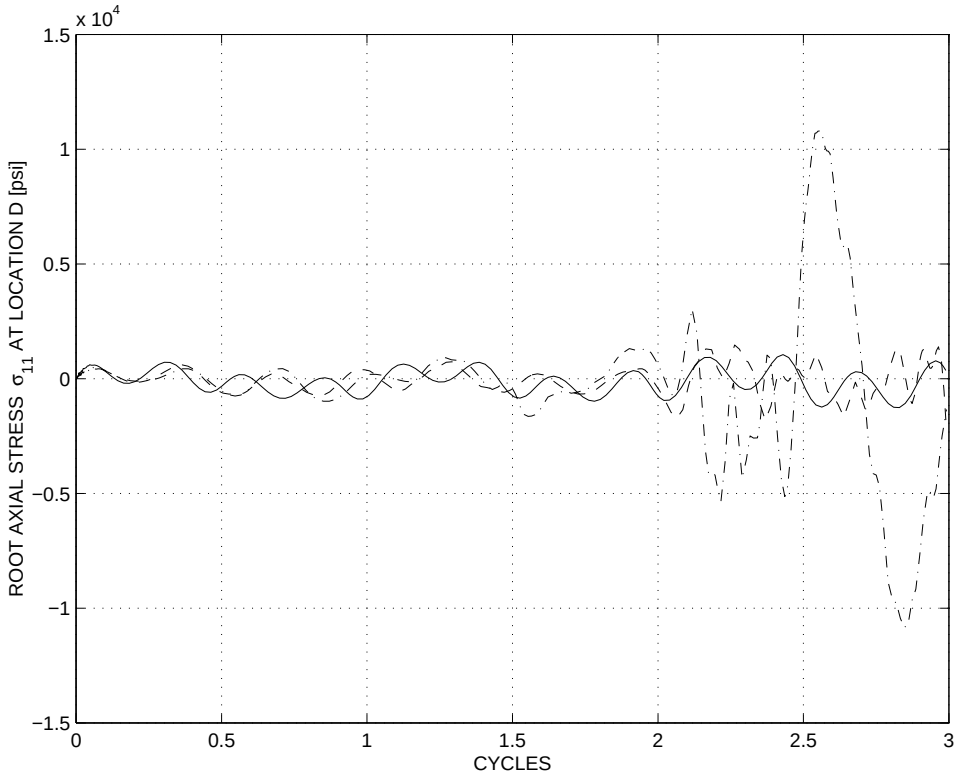

Figure 14: Time history of the link root axial stress σ_{11} at point D. *Lay-up 1*: solid line; *lay-up 2*: dashed line; *lay-up 3*: dashed-dot line.

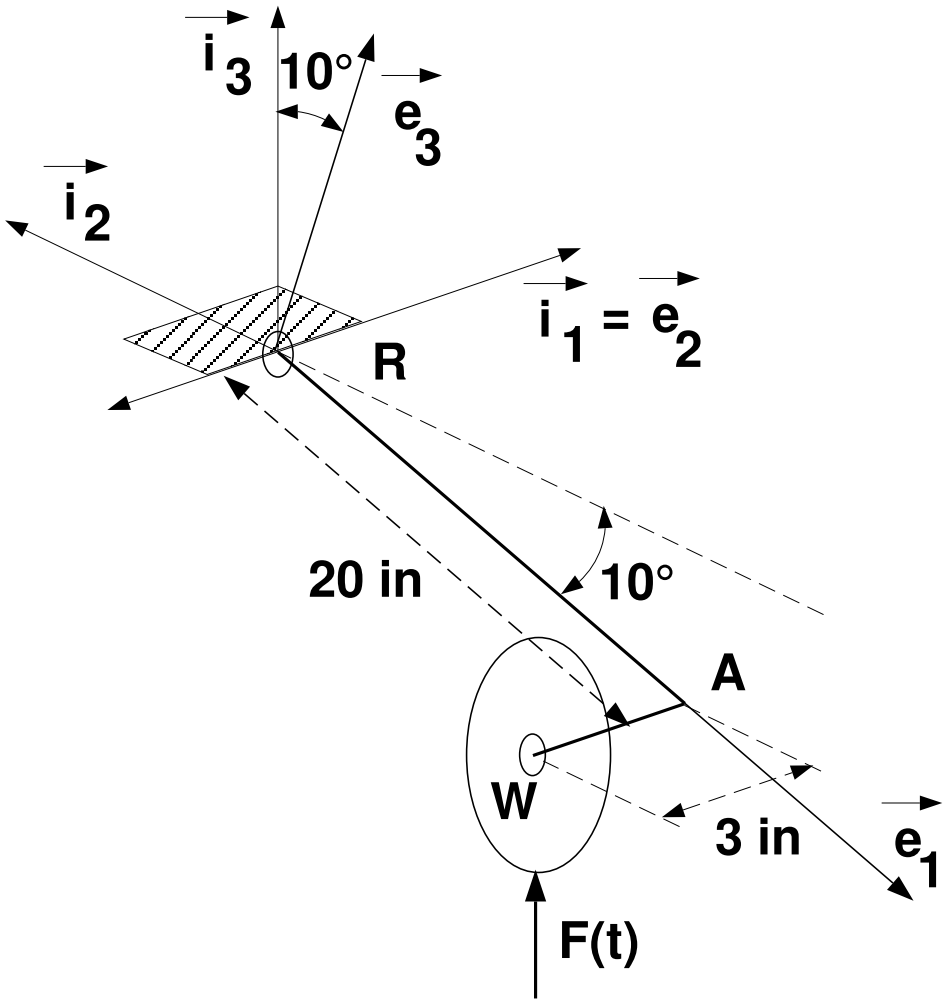

Figure 15: The suspension problem.

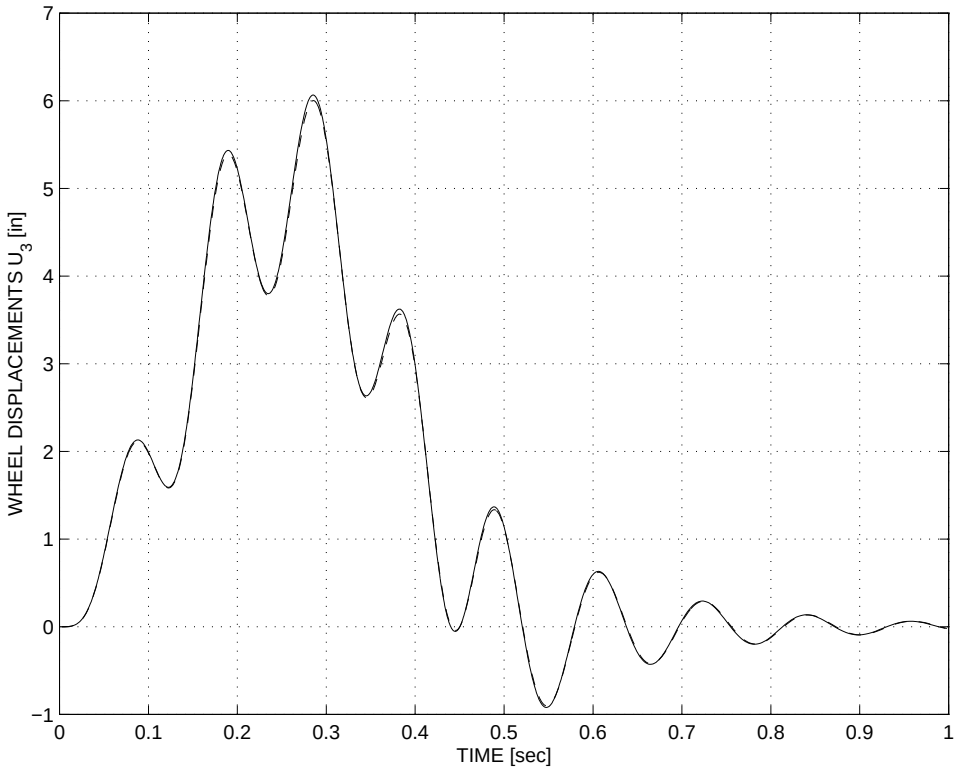

Figure 16: Time history of the wheel vertical displacement. *Lay-up 1*: solid line; *lay-up 3*: dashed line.

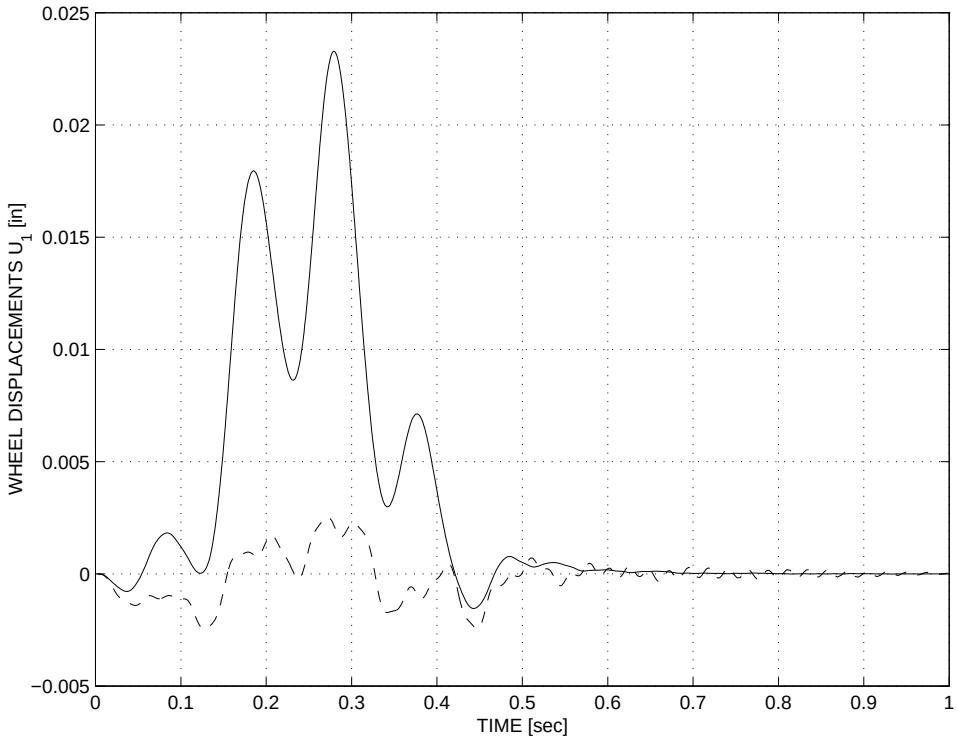

Figure 17: Time history of the wheel lateral displacement. *Lay-up 1*: solid line; *lay-up 3*: dashed line.

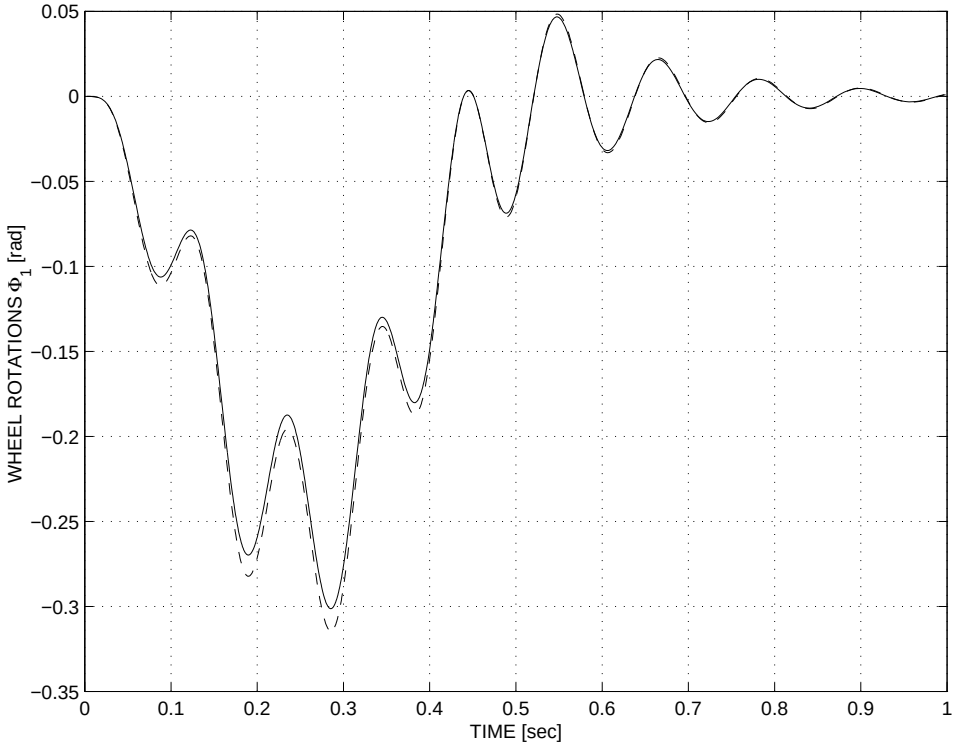

Figure 18: Time history of the wheel rotation ϕ_1. *Lay-up 1*: solid line; *lay-up 3*: dashed line.

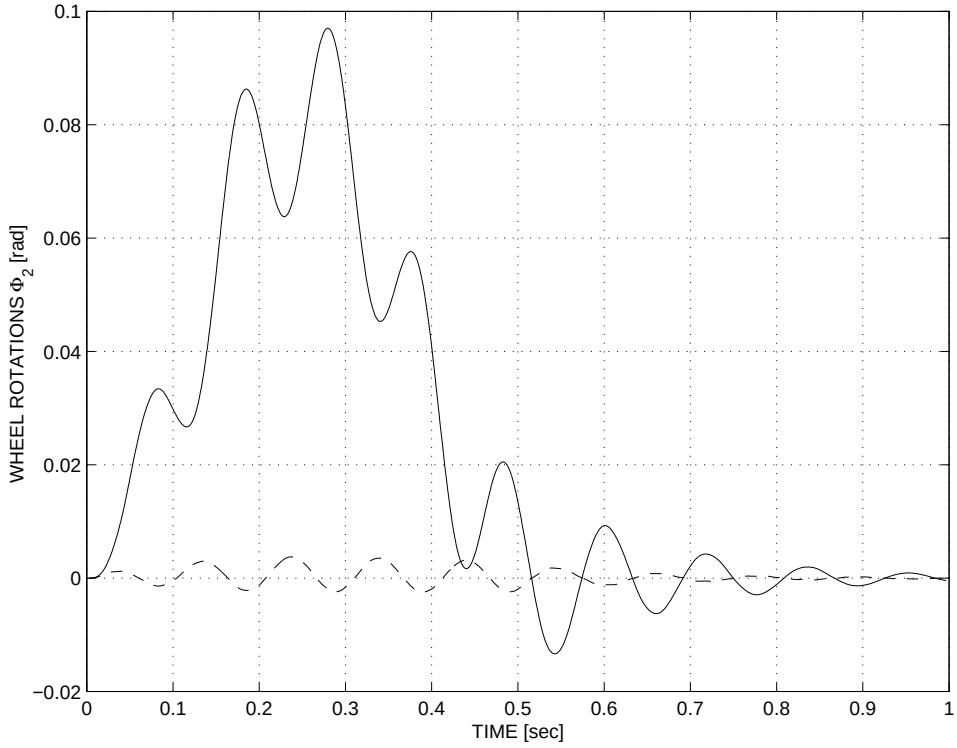

Figure 19: Time history of the wheel rotation ϕ_2. *Lay-up 1*: solid line; *lay-up 3*: dashed line.

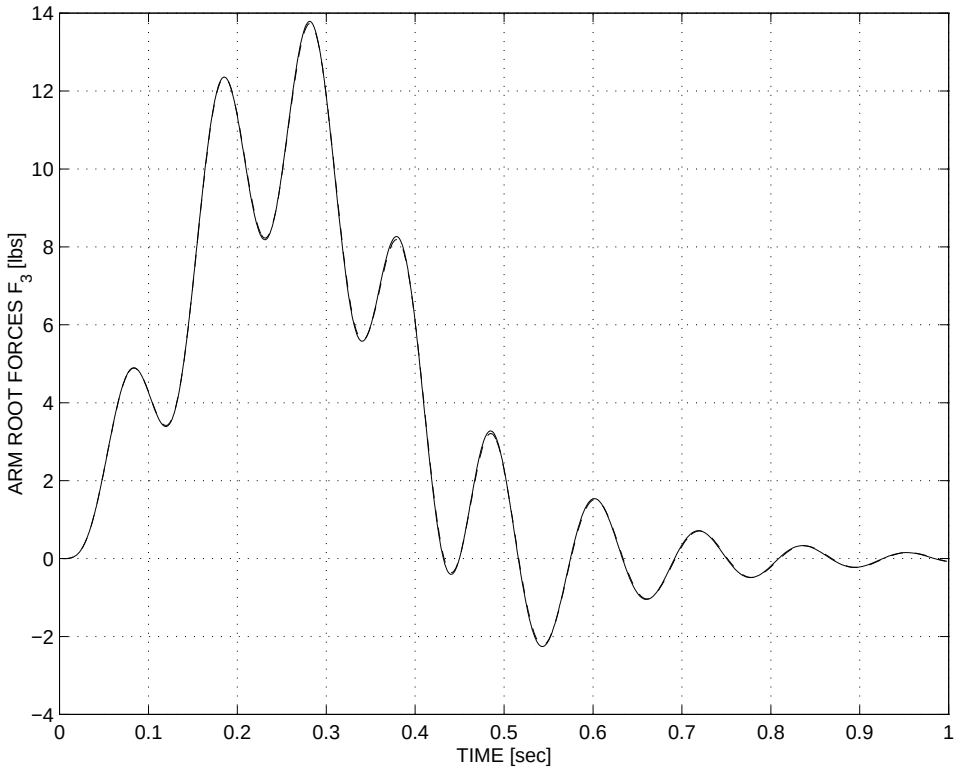

Figure 20: Time history of the arm root shear force F_3. *Lay-up 1*: solid line; *lay-up 3*: dashed line.

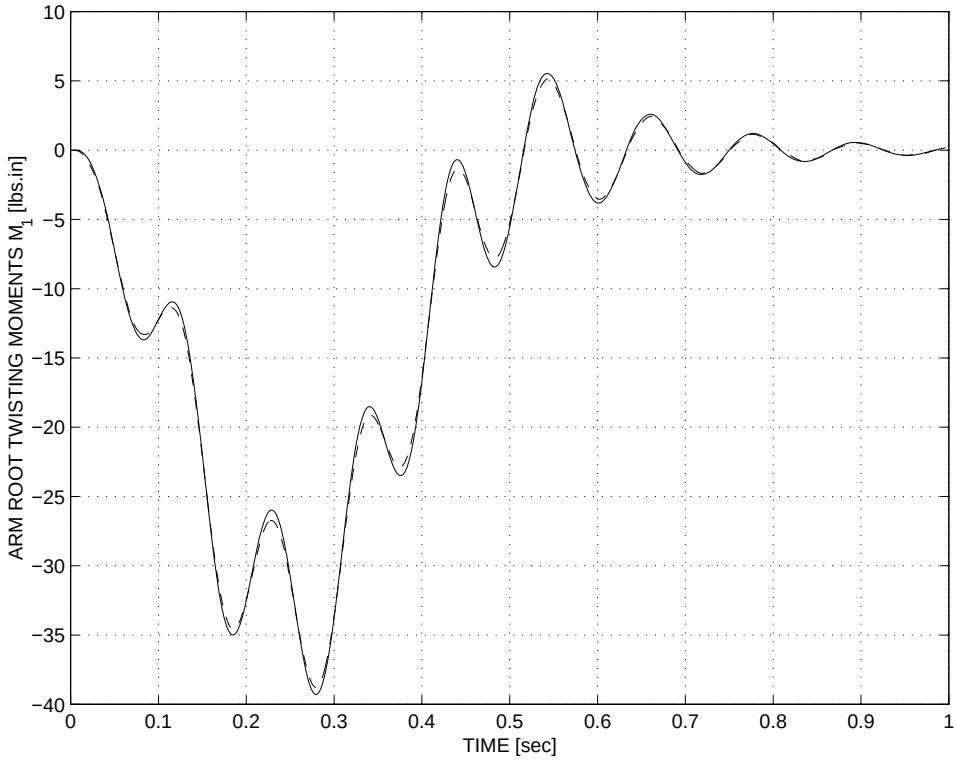

Figure 21: Time history of the arm root twisting moment M_1. *Lay-up 1*: solid line; *lay-up 3*: dashed line.

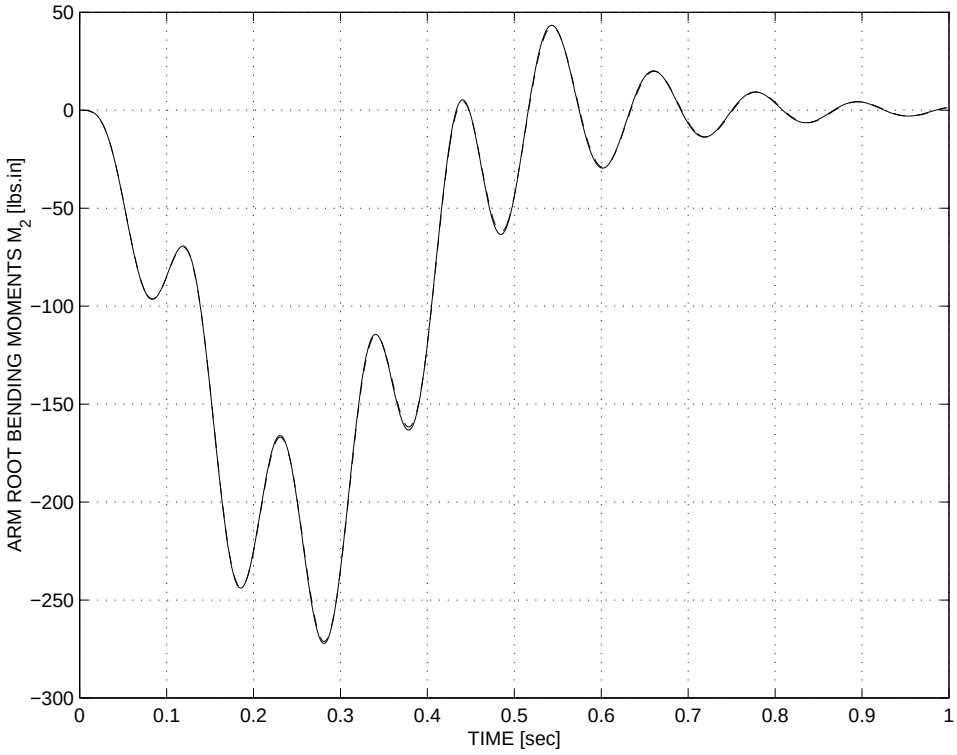

Figure 22: Time history of the arm root bending moment M_2. *Lay-up 1*: solid line; *lay-up 3*: dashed line.

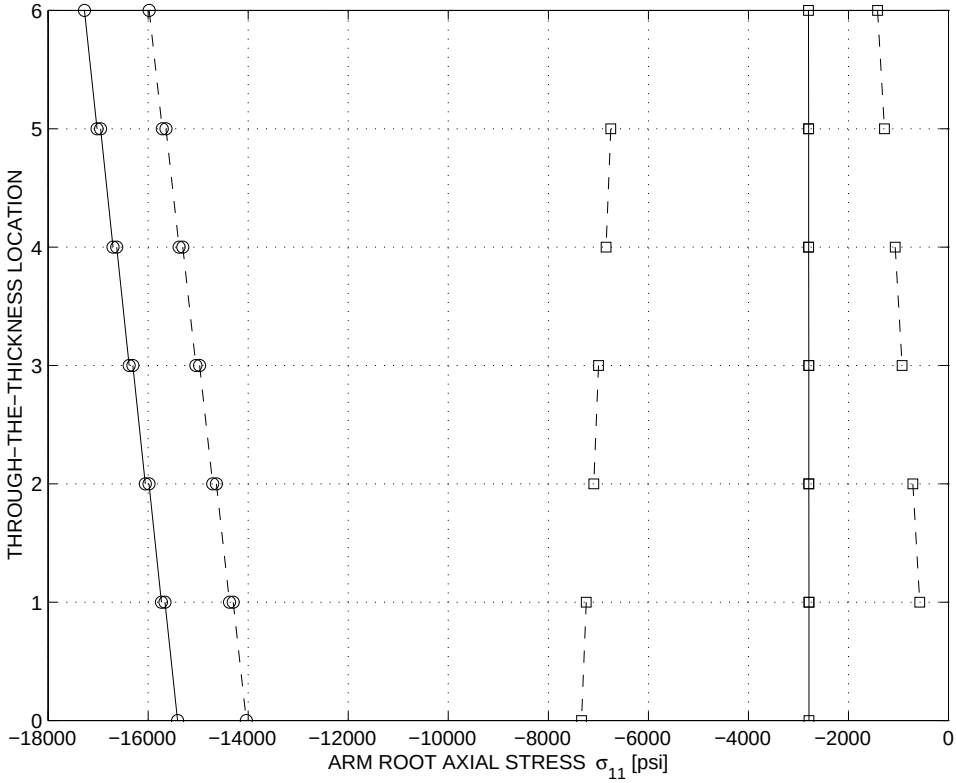

Figure 23: Distribution of root axial stresses through the thickness of the laminate. Location D: ($\circ$); Location E: ($\square$). *Lay-up 1*: solid line; *lay-up 3*: dashed line.

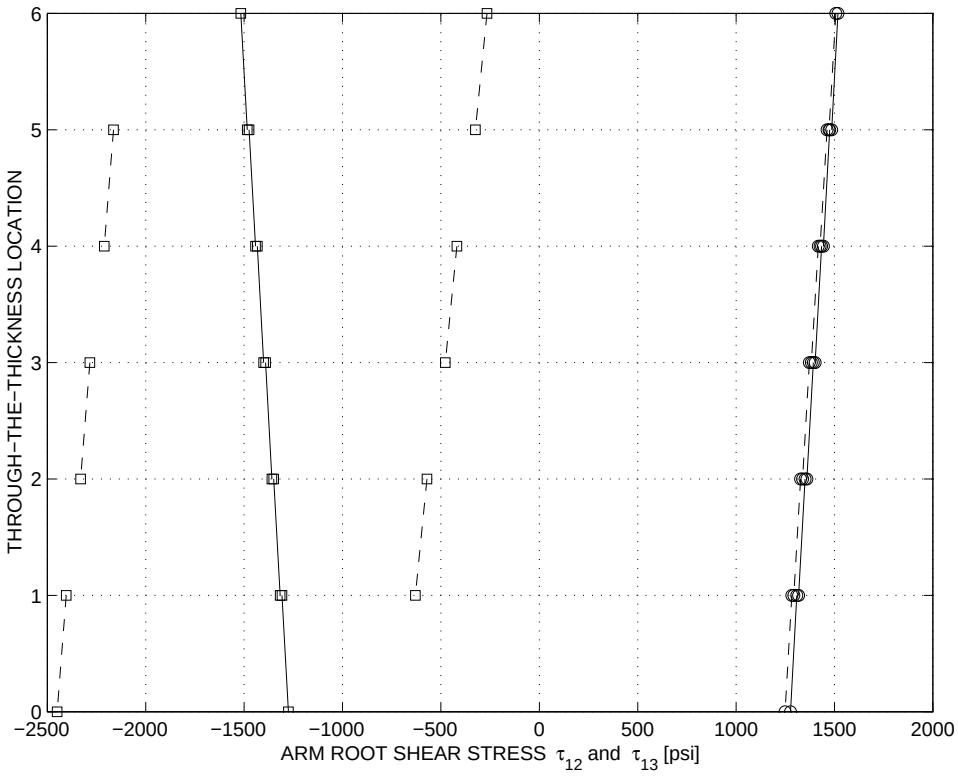

Figure 24: Distribution of root shear stresses through the thickness of the laminate. Shear stress τ_{12} at location D: ($\circ$); Shear stress τ_{13} at location E: ($\square$). *Lay-up 1*: solid line; *lay-up 3*: dashed line.

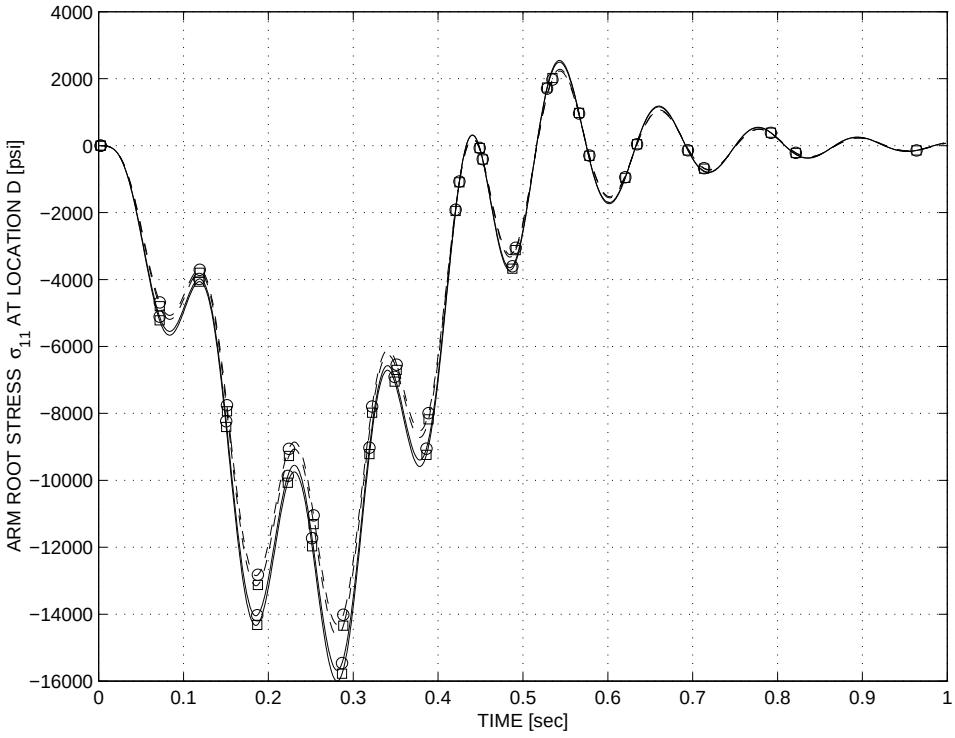

Figure 25: Time history root axial stresses σ_{11} in ply 1 ($\circ$) and ply 2 ($\square$) at location A. *Lay-up 1*: solid line; *lay-up 3*: dashed line.

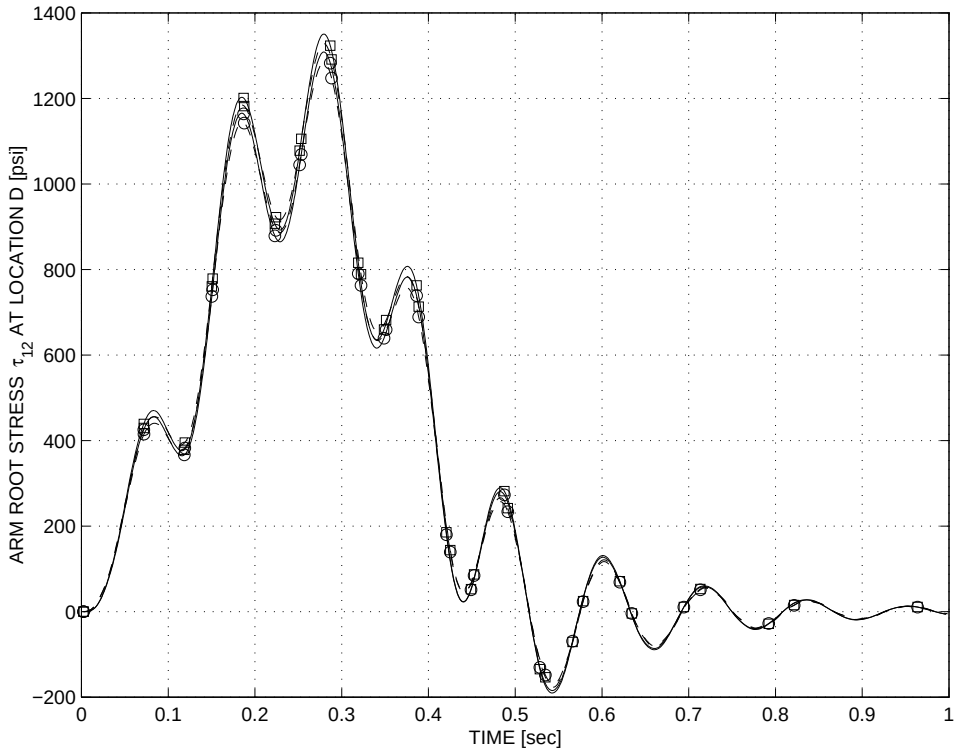

Figure 26: Time history root shear stresses τ_{12} in ply 1 ($\circ$) and ply 2 ($\square$). *Lay-up 1*: solid line; *lay-up 3*: dashed line.

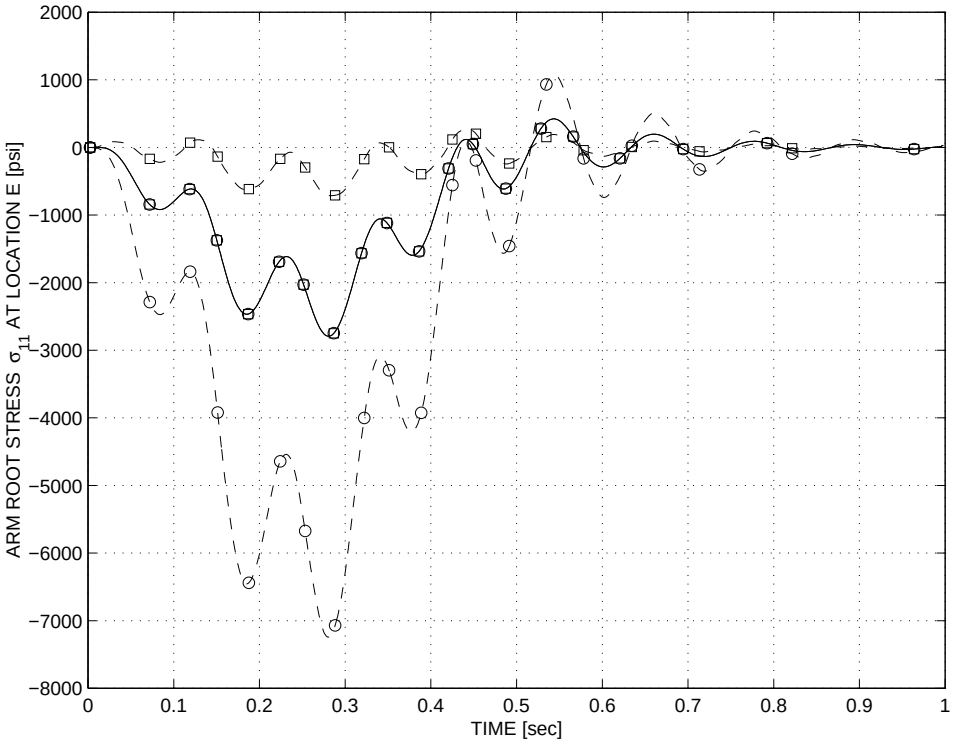

Figure 27: Time history root axial stresses σ_{11} in ply 1 ($\circ$) and ply 2 ($\square$) at location B. *Lay-up 1*: solid line; *lay-up 3*: dashed line.

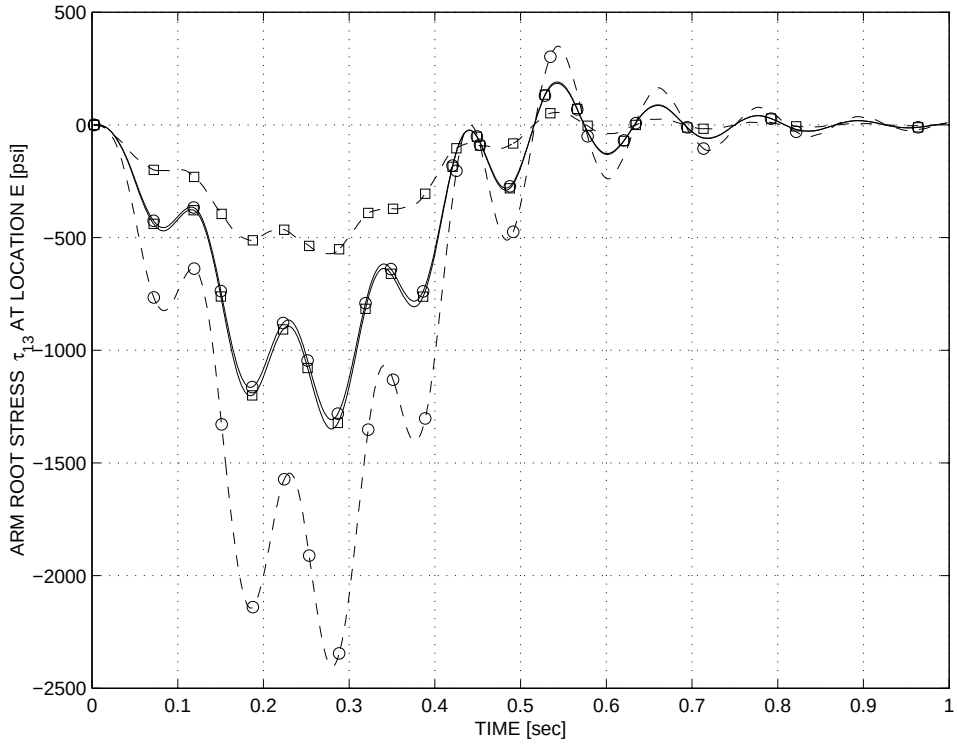

Figure 28: Time history root shear stresses τ_{13} in ply 1 (○) and ply 2 (□). *Lay-up 1*: solid line; *lay-up 3*: dashed line.